01.79.23

JOURNAL OF MAGNETIC RESONANCE 34, 515–535 (1979)

C.N.E.A. Biblioteca
ARCHIVO PUBLICACIONES
AÑO 1979
Nº 1

Theory of the Zeeman Effect of ^{14}N Nuclear Quadrupole Resonance with Polycrystalline Samples

SERGIO PISSANETZKY

Centro Atomico Bariloche, Comision Nacional de la Energia Atomica,
(8400) *San Carlos de Bariloche, Argentina**

Presented at the Fourth International Symposium on Nuclear Quadrupole Resonance, Osaka, Japan, September 1977

We present the true second-order theory of the Zeeman effect of the nuclear quadrupole resonance of nuclei with $I = 1$ with polycrystalline samples. In a previous publication [*J. Chem. Phys.* **59**, 4197 (1973)] an approximation was used and certain deviations were observed when comparing the results with the experimental points. The present theory gives excellent agreement with experiment for practically any nonzero value of the asymmetry parameter and for any value of the angle between the radiofrequency magnetic field and the Zeeman magnetic field. Thus, the results we present are the basis for the method for the identification of lines and the measurement of asymmetry parameters.

INTRODUCTION

Large polycrystalline samples are usually used to observe ^{14}N nuclear quadrupole resonance. The complete spectrum for each set of crystallographically equivalent ^{14}N sites consists of three lines: ν_+, ν_-, and ν_Δ. The gradient of the electric field at each site of an equivalent set is characterized by $eq \equiv \partial^2 V/\partial z^2 \equiv V_{zz}$ and $\eta \equiv (V_{xx} - V_{yy})/V_{zz}$. When at least two lines are detected for a set of sites, it is possible to calculate independently both parameters. However, in most cases only the ν_+ line is detected, or several ν_+ and ν_- lines are observed but cannot be assigned to sites. In such cases eq and η cannot be independently calculated.

The theory we present here is the basis for our method (*1*) which permits *both* parameters eq and η to be independently calculated by means of a Zeeman experiment performed on a *single* line, and to identify the line as a ν_+ or a ν_-. The Zeeman experiment consists of perturbing the observed line with a constant magnetic field and recording the observed frequency shift and reduction in amplitude of the line. This information together with the data on the unperturbed line is sufficient, in general, to identify the line and to furnish an approximate value of the asymmetry parameter η. Bounds can thus be set to the frequency of the other line of the pair ν_+, ν_- in order to save search time or to assign the lines of a complicated spectrum in pairs. If necessary a precise value of η can be obtained by performing careful measurements with different values of the perturbing field.

* Most of this work was done at the Facultad Experimental de Ciencias and Instituto de Investigaciones Petroleras, Universidad del Zulia, Maracaibo, Venezuela.

0022-2364/79/060515-21$02.00/0
Copyright © 1979 by Academic Press, Inc.
All rights of reproduction in any form reserved.
Printed in Great Britain

The theory also provides the basis for the interpretation of the patterns observed when the Zeeman modulation method is used for the detection of NQR absorptions. More information can be retrieved from an observed pattern if it is interpreted in the light of our results.

In a previous publication (Eq. [7] of Ref. (1)) the transition probabilities were calculated by using the unperturbed wavefunctions. A systematic deviation of the theoretical results from the experimental points was observed. The present theory produces a largely improved fitting with experiment in the region of interest. A small systematic deviation can be observed outside the region of interest and can be attributed to the assumption that the line shape is Gaussian.

THEORY

Our physical model is a nucleus of spin $I = 1$ and electric quadrupole moment Q interacting with an electric field gradient (efg) and perturbed by a constant magnetic field H applied at angles θ, Φ with respect to the principal set of axes of the efg tensor. Transitions are induced by a radiofrequency magnetic field $H'(t)$ applied at angles θ', Φ' with respect to the efg axes. Thus, we are going to deal with four Hamiltonians (*2*):

$$\begin{aligned}
\mathcal{H}_Q &= hK(3I_z^2 - I^2),\\
\mathcal{H}_\eta &= \eta hK(I_x^2 - I_y^2),\\
\mathcal{H}_M &= -g\mu_0 H(I_z\cos\theta + I_x\sin\theta\cos\Phi + I_y\sin\theta\sin\Phi),\\
\mathcal{H}_{RF}(t) &= -g\mu_0 H'(t)(I_z\cos\theta' + I_x\sin\theta'\cos\Phi' + I_y\sin\theta'\sin\Phi'),
\end{aligned} \tag{1}$$

where K is defined in Table 1.

$\mathcal{H}_Q$ is diagonal in the representation in which I_z and I^2 are diagonal. Thus, the angular momentum wavefunctions Ψ_{+1}, Ψ_{-1}, and Ψ_0 diagonalize $\mathcal{H}_Q$. The problem of diagonalizing $\mathcal{H}_Q + \mathcal{H}_\eta$ has a closed form solution (*3*). The wavefunctions are:

$$\begin{aligned}
\Psi_A &= (\Psi_{+1} + \Psi_{-1})/2^{1/2},\\
\Psi_B &= (\Psi_{+1} - \Psi_{-1})/2^{1/2},\\
\Psi_C &= \Psi_0,
\end{aligned} \tag{2}$$

and the transition frequencies are:

$$\begin{aligned}
\nu_+ &= (3+\eta)K \qquad (A \to C),\\
\nu_- &= (3-\eta)K \qquad (B \to C),\\
\nu_\Delta &= 2\eta K \qquad (A \to B).
\end{aligned} \tag{3}$$

$\mathcal{H}_M$ and $\mathcal{H}_{RF}$ are treated as perturbations. The first-order perturbations of the energies are zero for both Hamiltonians. Thus, second-order perturbation theory has to be used. We follow a procedure with several steps.

Step 1. The states A, B, and C are perturbed by $\mathcal{H}_M$. Second-order perturbation theory is used to calculate the energies $E_{A'}$, $E_{B'}$, and $E_{C'}$ and the wavefunctions $\Psi_{A'}$, $\Psi_{B'}$, and $\Psi_{C'}$ of the perturbed states A', B', and C'.

TABLE 1

DEFINITIONS OF SOME CONSTANTS AND VARIABLES USED IN THE TEXT

General definitions: $\lambda = \frac{3-\eta}{2\eta}$ $K = \frac{e^2Qq}{4h}$ $D = \frac{g\mu_0 H}{h}$ $\mu = \frac{3}{2}\cos^2\alpha - \frac{1}{2}$

Symbol	Definition for transition 1	Definition for transition 2	Definition for transition 3
ν_0	$(3+\eta)K$	$(3-\eta)K$	$2\eta K$
ν	ν_1	ν_2	ν_3
T	$\lambda - 2U$	$\lambda + 1 - 2U$	$-2U$
U	$-1 - \frac{1}{\lambda - 1}$	$1 - \frac{1}{\lambda + 2}$	$-\frac{\lambda}{2} - \frac{1}{4} + \frac{1}{4(2\lambda+1)}$
W_1	$\frac{3}{\pi}\frac{\lambda}{\lambda-1}\cos^2\alpha$	$\frac{3}{2\pi}\frac{\lambda+1}{\lambda+2}\sin^2\alpha$	$\frac{3}{2\pi}\frac{\lambda(\lambda+1)}{2\lambda+1}\sin^2\alpha$
W_2	$-\lambda W_3$	$-(\lambda+1)W_3$	0
W_3	$-\frac{3}{\pi}\frac{\mu}{\lambda-1}$	$\frac{3}{\pi}\frac{\mu}{\lambda+2}$	$\frac{3}{\pi}\frac{\mu}{2\lambda+1}$
W_4	W_3	0	$(\lambda+1)W_3$
W_5	0	$\frac{12}{\pi}\frac{\lambda+1}{\lambda+2}\cos^2\alpha$	0
W_6	$-4W_1$	0	0
W_7	$-\frac{3\mu}{\pi}\left(2\lambda+5+\frac{1}{\lambda}\right)$	$\frac{3\mu}{\pi}\left(2\lambda-3+\frac{1}{\lambda+1}\right)$	$-\frac{3\mu}{\pi}\left(\frac{1}{\lambda+1}+\frac{1}{\lambda}\right)$
W_8	$\frac{3}{\pi}\left[\frac{4\cos^2\alpha}{\lambda-1}+\mu\left(1-\frac{1}{\lambda}\right)\right]$	$\frac{-3}{\pi(\lambda+2)}\left[2\sin^2\alpha+\frac{\mu\lambda^2(\lambda+3)}{(\lambda+1)^2}\right]$	$\frac{-3}{\pi(2\lambda+1)}\left(2\sin^2\alpha+\mu\frac{3\lambda+1}{\lambda(\lambda+1)^2}\right)$
W_9	$\frac{6\mu}{\pi}\left(1+\frac{1}{\lambda}\right)^2$	$-\frac{6\mu}{\pi}\frac{\lambda^2}{(\lambda+1)^2}$	$\frac{6}{\pi}\frac{\mu}{\lambda^2(\lambda+1)^2}$
W_{10}	$(\lambda+1)(W_8-W_9)$	$W_5+(\lambda+1)(W_8-W_9)$	$(\lambda+1)(W_8-W_9)$
W_{11}	$W_7+(\lambda+1)W_9$	$W_7+(\lambda+1)W_9$	$W_7+(\lambda+1)W_9$
$\frac{\nu_{\min}\nu_0}{D^2}$	$1+1/\lambda$	$-\lambda$	$-1/\lambda$
$\frac{\nu_{\max}\nu_0}{D^2}$	$\lambda+1$	2	2

Step 2. The states A′, B′, and C′ are perturbed by $\mathcal{H}_{RF}(t)$. The wavefunctions $\Psi_{A'}$, $\Psi_{B'}$, and $\Psi_{C'}$ are used to calculate the probabilities of the transitions induced by the time-dependent Hamiltonian $\mathcal{H}_{RF}(t)$.

Step 3. The effect of the polycrystalline sample is considered. The angles θ, Φ, θ' and Φ' are different for different microcrystals. The efg set of axes is abandoned and the problem is treated from a laboratory frame defined by H and H'. The only constant angle is α, the angle between H and H'. The line shape is computed by adding up the contributions, at each frequency, of all the microcrystals.

Step 4. Several algebraic or numeric tests are implemented on both the intermediate and final results. Such tests are necessary to check the results because of the very involved algebra of steps 2 and 3.

Step 5. We consider absorption lines with finite width.

The main difference of the present theory with our previous formulation (1) is in step 2. In the previous formulation the probabilities of the transitions induced by $\mathcal{H}_{RF}$ were calculated by using the unperturbed wavefunctions Ψ_A, Ψ_B and Ψ_C.

PERTURBED ENERGIES AND WAVEFUNCTIONS

When $\mathcal{H}_Q + \mathcal{H}_\eta$ is perturbed by $\mathcal{H}_M$, the second-order perturbed energies are (3):

$$\begin{aligned}
\frac{E_{A'}}{h} &= (1+\eta)K + \frac{D^2\cos^2\theta}{2\eta K} + \frac{D^2\sin^2\theta\cos^2\Phi}{(3+\eta)K},\\
\frac{E_{B'}}{h} &= (1-\eta)K - \frac{D^2\cos^2\theta}{2\eta K} + \frac{D^2\sin^2\theta\sin\Phi}{(3-\eta)K},\\
\frac{E_{C'}}{h} &= -2K - \frac{D^2\sin^2\theta\cos^2\Phi}{(3+\eta)K} - \frac{D^2\sin^2\theta\sin^2\Phi}{(3-\eta)K},
\end{aligned} \qquad [4]$$

where D is defined in Table 1. After some calculations, expressions [4] can be written:

$$\begin{aligned}
\frac{E_{A'}}{h} &= (1+\eta)K + \frac{D^2}{(3+\eta)K}\left[\frac{3+\eta}{2\eta} - \sin^2\theta\left(\frac{3-\eta}{2\eta} + \sin^2\Phi\right)\right],\\
\frac{E_{B'}}{h} &= (1-\eta)K + \frac{D^2}{(3-\eta)K}\left[-\frac{3-\eta}{2\eta} + \sin^2\theta\left(\frac{3-\eta}{2\eta} + \sin^2\Phi\right)\right],\\
\frac{E_{C'}}{h} &= -2K - \frac{D^2}{(3+\eta)K}\,\frac{2\eta}{3-\eta}\sin^2\theta\left(\frac{3-\eta}{2\eta} + \sin^2\Phi\right).
\end{aligned} \qquad [5]$$

The form of these expressions suggests the definition of the constant:

$$\lambda = (3-\eta)/2\eta \qquad [6]$$

and has the advantage that the functional dependence on the angles θ and Φ can be expressed by a single function:

$$v(\theta, \Phi) = \sin^2\theta(\lambda + \sin^2\Phi), \qquad [7]$$

where

$$0 \le v(\theta, \Phi) \le \lambda + 1. \qquad [8]$$

The energy levels can now be written in terms of λ and $v(\theta, \Phi)$:

$$\begin{aligned}
\frac{E_{A'}}{h} &= (1+\eta)K + \frac{D^2}{(3+\eta)K}(\lambda + 1 - v(\theta, \Phi)),\\
\frac{E_{B'}}{h} &= (1-\eta)K + \frac{D^2}{(3-\eta)K}(-\lambda + v(\theta, \Phi)),\\
\frac{E_{C'}}{h} &= -2K - \frac{D^2}{(3+\eta)K}v(\theta, \Phi)/\lambda.
\end{aligned} \qquad [9]$$

We call $\nu_{A'C'}$, $\nu_{B'C'}$, and $\nu_{A'B'}$ the frequencies of the transitions between the corresponding perturbed levels and we define the frequency shifts produced by the perturbation:

$$\begin{aligned} \nu_1 &= \nu_{A'C'} - \nu_+, \\ \nu_2 &= \nu_{B'C'} - \nu_-, \\ \nu_3 &= \nu_{A'C'} - \nu_\Delta. \end{aligned} \tag{10}$$

Using Eqs. [9] and [3], the frequency shifts [10] can be expressed in the following nondimensional form:

$$\begin{aligned} \frac{\nu_1 \nu_+}{D^2} &= \lambda + 1 + \left(\frac{1}{\lambda} - 1\right) v(\theta, \Phi), \\ \frac{\nu_2 \nu_-}{D^2} &= -\lambda + \left(1 + \frac{1}{\lambda + 1}\right) v(\theta, \Phi), \\ \frac{\nu_3 \nu_\Delta}{D^2} &= 2 - \left(\frac{1}{\lambda} + \frac{1}{\lambda + 1}\right) v(\theta, \Phi). \end{aligned} \tag{11}$$

The simplicity of these expressions has encouraged us to proceed with the algebraically complicated calculations of the next paragraph.

Up to this point our formulation has led us to consider the frequency shifts ν_1, ν_2 and ν_3 as functions of the parameter v, which is in turn a function of the angles θ and Φ. However, Eq. [7] will be used to express Φ as a function of θ and of v, where v is in turn expressed as a function of ν_1, ν_2, or ν_3 with the help of Eq. [11]. Furthermore, one of our goals is to identify an observed absorption line whose unperturbed central frequency ν_0 has been measured, but it is unknown whether ν_0 is a ν_+, a ν_-, or a ν_Δ. We thus reformulate Eq. [11] for all three lines in the following way:

$$v(\nu) = T + U\nu\nu_0/D^2, \tag{12}$$

where ν stands for ν_1, ν_2, or ν_3, and ν_0 stands for ν_+, ν_-, or ν_Δ, and the constants T and U depend only on the asymmetry parameter η but have different expressions for each of the three transitions. See Table 1.

We now reformulate Eq. [7]. We define:

$$x = \cos\theta \tag{13}$$

and we have

$$\begin{aligned} \sin^2\theta \sin^2\Phi &= v(\nu) - \lambda + \lambda x^2, \\ \sin^2\theta \cos^2\Phi &= \lambda + 1 - v(\nu) - (\lambda + 1)x^2. \end{aligned} \tag{14}$$

We have also used the second-order perturbation theory to compute the matrix $\mathcal{U}$ of the unitary transformation from the representation in which $\mathcal{H}_Q + \mathcal{H}_\eta$ is diagonal to the representation in which $\mathcal{H}_Q + \mathcal{H}_\eta + \mathcal{H}_M$ is diagonal up to the second order of approximation in the perturbation D. The matrix $\mathcal{U}$ is needed for step 2. Its

expression is:

$$\mathcal{U} = \begin{vmatrix} 1-\frac{a^2}{2\beta^2}-\frac{b^2}{2\gamma^2} & -\frac{b}{\gamma}-\frac{iac}{\beta\gamma} & -\frac{a}{\beta}+\frac{ibc}{\beta\gamma} \\ \frac{b}{\beta}-\frac{iac}{\gamma\delta} & 1-\frac{b^2}{2\gamma^2}-\frac{c^2}{2\delta^2} & -\frac{ic}{\delta}-\frac{ab}{\gamma\delta} \\ \frac{a}{\beta}-\frac{ibc}{\beta\delta} & -\frac{ic}{\delta}+\frac{ab}{\beta\delta} & 1-\frac{a^2}{2\beta^2}-\frac{c^2}{2\delta^2} \end{vmatrix}, \qquad [15]$$

where:

$$\begin{aligned} a &= D \sin\theta \cos\Phi, \\ b &= D \cos\theta, \\ c &= D \sin\theta \sin\Phi, \end{aligned} \qquad [16]$$

and:

$$\begin{aligned} \beta &= (3+\eta)K, \\ \gamma &= 2\eta K, \\ \delta &= (3-\eta)K. \end{aligned} \qquad [17]$$

The second-order perturbed wavefunctions are thus

$$\begin{vmatrix} \Psi_{A'} \\ \Psi_{B'} \\ \Psi_{C'} \end{vmatrix} = \mathcal{U} \begin{vmatrix} \Psi_A \\ \Psi_B \\ \Psi_C \end{vmatrix}. \qquad [18]$$

We have checked the above results. The matrix $\mathcal{U}$ is unitary, as it should be, and the wavefunctions $\Psi_{A'}$, $\Psi_{B'}$, and $\Psi_{C'}$ do in fact diagonalize $\mathcal{H}_Q + \mathcal{H}_\eta + \mathcal{H}_M$ up to the second order in D, and give the eigenvalues of Eq. [4].

TRANSITION PROBABILITIES

We are now ready for step 2. $\mathcal{H}_{RF}$ is considered as a time-dependent perturbation of the system represented by $\mathcal{H}_Q + \mathcal{H}_\eta + \mathcal{H}_M$. We first write the matrix of $\mathcal{H}_{RF}$ in the representation in which $\mathcal{H}_Q + \mathcal{H}_\eta$ is diagonal. We keep only the angular part because we are only interested in *relative* changes of the amplitude of the absorption line, and we introduce the constant $(8\pi^2/3)^{1/2}$, which corresponds, in our formulation, to the amplitude of the unperturbed line. We have:

$$\mathcal{H}_{RF} = \begin{vmatrix} 0 & p & q \\ p & 0 & -ir \\ q & ir & 0 \end{vmatrix}, \qquad [19]$$

where

$$p = (8\pi^2/3)^{-1/2} \cos\theta',$$
$$q = (8\pi^2/3)^{-1/2} \sin\theta' \cos\Phi', \qquad [20]$$
$$r = (8\pi^2/3)^{-1/2} \sin\theta' \sin\Phi'.$$

We now perform a unitary transformation on the matrix of $\mathcal{H}_{RF}$ of Eq. [19] by means of the conjugate and the transpose of the matrix $\mathcal{U}$ of Eq. [15]. The result is the matrix of $\mathcal{H}_{RF}$ in the representation in which $\mathcal{H}_Q + \mathcal{H}_\eta + \mathcal{H}_M$ is diagonal, which is our basic representation for all the calculations which follow. Then, we calculate the squares of the absolute values of the off-diagonal elements of the resulting matrix, which are proportional to the transition probabilities. We obtain:

$$|(\mathcal{H}_{RF})_{A'B'}|^2 = p^2\left(1 - \frac{4a^2}{\beta^2} - \frac{b^2}{\gamma^2} - \frac{c^2}{\delta^2}\right) + q^2\frac{c^2}{\delta^2} + r^2\frac{b^2}{\beta^2} + \frac{2pa}{\beta}\left(\frac{1}{\delta} - \frac{1}{\gamma}\right)(qb - rc) - 2qr\frac{bc}{\gamma\delta},$$

$$|(\mathcal{H}_{RF})_{A'C'}|^2 = p^2\frac{c^2}{\delta^2} + q^2\left(1 - \frac{a^2}{\beta^2} - \frac{4b^2}{\gamma^2} - \frac{c^2}{\delta^2}\right) + r^2\frac{a^2}{\beta^2} + \frac{2qb}{\gamma}\left(\frac{1}{\beta} + \frac{1}{\delta}\right)(rc - pa) + 2pr\frac{ac}{\beta\delta},$$

$$|(\mathcal{H}_{RF})_{B'C'}|^2 = p^2\frac{b^2}{\gamma^2} + q^2\frac{a^2}{\beta^2} + r^2\left(1 - \frac{a^2}{\beta^2} - \frac{b^2}{\gamma^2} - \frac{4c^2}{\delta^2}\right) + \frac{2rc}{\delta}\left(\frac{1}{\beta} + \frac{1}{\gamma}\right)(qb - pa) + 2pq\frac{ab}{\beta\gamma}. \qquad [21]$$

For the sake of brevity we use $P(\theta, \Phi, \theta', \Phi')$ as a common name for the three expressions [21].

In fact, we have also calculated the squares of the absolute values of the diagonal terms in order to be able to check the algebra of Eq. [21] by means of the well-known property which states that the sum of the squares of the absolute values of all the elements of a matrix is invariant after a unitary transformation. This property has been verified at several stages of the calculations and has been of great help for the detection of algebraic mistakes. We are now ready for step 3.

THE POLYCRYSTALLINE SAMPLE

Now we regard the situation from the laboratory frame defined by H and H', see Fig. 1. The angle α between H and H' is the only angle which is fixed and given. We think of the polycrystalline sample as if it consisted of a large set of resonant nuclei, to each of which we attach the "nuclear" frame x, y, z defined by the principal axes of the efg tensor at the site of the nucleus. We make the following assumptions:

(i) The distribution of all the z-axes is uniform on the unit sphere.

(ii) Given a point on the unit sphere, all nuclei which have their z-axes passing near the point also have their x- (or y-) axes uniformly distributed about z.

We recall that the angular coordinates of H with respect to the nuclear frame are θ, Φ, and those of H' are θ', Φ'. The angular coordinates of H' in the laboratory frame are α, 0, and those of z are θ, ϕ. The x- and y-axes of the nuclear frame are not shown in Fig. 1, however, the angle Φ determines the rotation of the x-axis with respect to the laboratory frame.

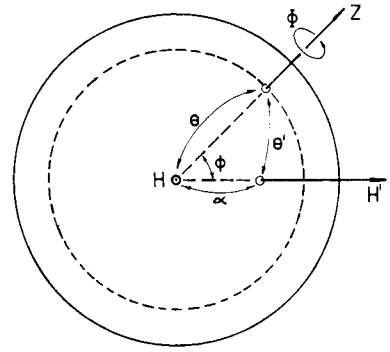

FIG. 1. The unit sphere and the Laboratory frame of reference. H is the Zeeman magnetic field and H' is the radiofrequency magnetic field at an angle α with H. x, y, and z are the principal axes of the efg tensor; however, only z is indicated for clarity.

The transition probabilities are proportional to $P(\theta, \Phi, \theta', \Phi')$, given by Eq. [21]. The angles θ' and Φ' are given as functions of θ, Φ, ϕ, and α by the following identities:

$$\begin{aligned} \sin\theta' \cos(\Phi' - \Phi) &= \sin\theta \cos\alpha - \cos\theta \sin\alpha \cos\phi, \\ \sin\theta' \sin(\Phi' - \Phi) &= \sin\alpha \sin\phi, \\ \cos\theta' &= \cos\alpha \cos\theta + \sin\alpha \sin\theta \cos\phi. \end{aligned} \qquad [22]$$

With the help of these identities we express P as a function of θ, Φ, ϕ, and α:

$$P(\theta, \Phi, \phi, \alpha) = P\{\theta, \Phi, \theta'(\theta, \Phi, \phi, \alpha), \Phi'(\theta, \Phi, \phi, \alpha)\}. \qquad [23]$$

The number of nuclei whose z-axes fall within some $d\theta$ and some $d\phi$, and whose azimuth is within some $d\Phi$, is proportional to $\sin\theta\, d\theta\, d\phi\, d\Phi$. For a given H, all such nuclei absorb energy at a frequency $\nu(\theta, \Phi)$ given by Eq. [11]. The intensity of the absorption at this frequency is thus proportional to:

$$P(\theta, \Phi, \phi, \alpha) \sin\theta\, d\theta\, d\phi\, d\Phi. \qquad [24]$$

THE TOTAL ABSORPTION OF ENERGY AT A GIVEN FREQUENCY

We want to calculate the total energy absorbed by all the nuclei at a *given* frequency ν measured from the center of the corresponding unperturbed line. As ν is independent of ϕ (see Eqs. [11]) we start by adding up the contributions of all the nuclei with the same θ and Φ but with all possible values of ϕ:

$$P(\theta, \Phi, \alpha) \sin\theta\, d\theta\, d\Phi = \int_{\phi=0}^{2\pi} d\phi\, P(\theta, \Phi, \phi, \alpha) \sin\theta\, d\theta\, d\Phi. \qquad [25]$$

Equations [11] give the frequency ν as a function of the parameter v which is in turn a function of θ and Φ. As ν is now given, we use Eq. [12] to express the parameter v as a function of ν, and then choose Φ as the dependent variable and express it as a

function of v and θ by means of Eqs., [14]. We also have:

$$d\Phi = \{\partial\Phi(\theta, \nu)/\partial\nu\}\, d\nu. \qquad [26]$$

Using [26], [12], and [14] in [25] we calculate:

$$P(\theta, \nu, \alpha) \sin\theta\, d\theta\, d\nu = 4P\{\theta, \Phi(\theta, \nu), \alpha\} \sin\theta\, d\theta \{\partial\Phi(\theta, \nu)/\partial\nu\}\, d\nu. \qquad [27]$$

The factor 4 comes from the fact that the function $\Phi(\theta, \nu)$ is multivalued and has four branches.

Finally we note that there is a whole range of values of θ for which a contribution to the absorption at a given frequency ν will exist. From the definition of v, Eq. [7], we have for all possible values of the dependent variable Φ:

$$\frac{v}{\lambda + 1} \leq \sin^2\theta \leq \frac{v}{\lambda}, \qquad [28]$$

where v can take on values only in the range given by Eq. {8}. We define $\theta_{\min}$ and $\theta_{\max}$ by:

$$\begin{aligned} \sin^2\theta_{\min} &= \frac{v}{\lambda + 1}, \\ \sin^2\theta_{\max} &= \mathrm{Min}(1, v/\lambda). \end{aligned} \qquad [29]$$

Each of Eqs. [29] has two solutions when $0 \leq \theta \leq \pi$. We take the solutions which are less than $\pi/2$ and integrate over the range so defined, multiplying the result by 2:

$$P(\nu, \alpha)\, d\nu = 2 \int_{\theta=\theta_{\min}(\nu)}^{\theta_{\max}(\nu)} d\theta\, P(\theta, \nu, \alpha) \sin\theta\, d\nu. \qquad [30]$$

Thus, the amplitude of the perturbed absorption line will be proportional to $P(\nu, \alpha)$.

All the calculations required to obtain the explicit expressions of $P(\nu, \alpha)$ for the three lines are straightforward, except for the extremely intricate algebra involved. The integrations in Eq. [25] are very simple. The integrations in Eq. [30] require the use of the elliptic integrals of the first and second kind:

$$\begin{aligned} K(k) &= \int_0^{\pi/2} (1 - k^2 \sin^2\beta)^{-1/2}\, d\beta, \\ E(k) &= \int_0^{\pi/2} (1 - k^2 \sin^2\beta)^{1/2}\, d\beta, \end{aligned} \qquad [31]$$

where:

$$k^2 = \frac{v}{\lambda(\lambda + 1 - v)}. \qquad [32]$$

The final result is:

$$(D^2/\nu_0)P(\nu,\alpha)=J_A+(D^2/\nu_0^2)J_B, \qquad [33]$$

where J_A and J_B are functions of $(\nu\nu_0/D^2)$ and of α alone (and of course of the given value of the asymmetry parameter η). J_A and J_B are defined differently for the ranges $0\le v<\lambda$ and $\lambda<v\le\lambda+1$. For $v=\lambda$, $k^2=1$, and $K(k)$ is logarithmically divergent. This poses no problems except for the numerical integration which will be required later. The definitions of J_A and J_B follow.

For $0\le v<\lambda$:

$$\begin{aligned} J_A&=\{\lambda(\lambda+1-v)\}^{-1/2}\{W_1+W_2(\lambda-v)\}K(k)+W_3\{\lambda(\lambda+1-v)\}^{1/2}E(k),\\ J_B&=\{W_5(\lambda-v)(\lambda+1-v)^{-1/2}+W_6(\lambda+1-v)^{1/2}\\ &\quad+W_7(\lambda-v)(\lambda+1-v)^{1/2}\}\lambda^{-1/2}K(k)+\{\lambda(\lambda+1-v)\}^{1/2}\{W_8+W_9(\lambda-v)\}E(k). \end{aligned} \qquad [34]$$

For $\lambda<v\le\lambda+1$:

$$\begin{aligned} J_A&=\{W_1+W_4(\lambda-v)\}v^{-1/2}K(1/k)+W_3v^{1/2}E(1/k),\\ J_B&=\{W_{10}(\lambda-v)+W_6(\lambda+1-v)+W_{11}(\lambda-v)(\lambda+1-v)\}v^{-1/2}K(1/k)\\ &\quad+v^{1/2}\{W_8+W_9(\lambda-v)\}E(1/k). \end{aligned} \qquad [35]$$

These definitions are valid for all three lines. The constants W_i depend only on α and η, but have different expressions for each line. They are given in Table 1. The expressions are given in the form which is best suited for computer programming.

THE TOTAL RELATIVE ENERGY ABSORBED BY THE SAMPLE

By integration of Eq. [23] we can calculate the total energy absorbed at all frequencies of each perturbed line by all the nuclei:

$$P(\alpha)=\int_0^{2\pi}d\phi\int_0^{2\pi}d\Phi\int_0^{\pi}d\theta\,\sin\theta P(\theta,\Phi,\phi,\alpha). \qquad [36]$$

After some algebraic expansions we obtain, for the three lines:

$$\begin{aligned} P_1(\alpha)&=1+\frac{D^2}{\nu_0^2}\left\{-4\cos^2\alpha+\frac{2}{5}\mu\left(4-\frac{(\lambda+1)^2}{\lambda}\right)\right\},\\ P_2(\alpha)&=1+\frac{D^2}{\nu_0^2}\left\{-2\sin^2\alpha+\frac{2}{5}\mu\left(\frac{\lambda^2}{\lambda+1}-6\right)\right\},\\ P_3(\alpha)&=1+\frac{D^2}{\nu_0^2}\left\{-2\sin^2\alpha+\frac{2}{5}\mu\left(\frac{1}{\lambda(\lambda+1)}-6\right)\right\}, \end{aligned} \qquad [37]$$

where μ is defined in Table 1.

When $D=0$, all three energies are equal to 1. This is so because the appropriate constant $(8\pi^2/3)^{1/2}$ was introduced in Eq. [20]. We are only interested in calculating

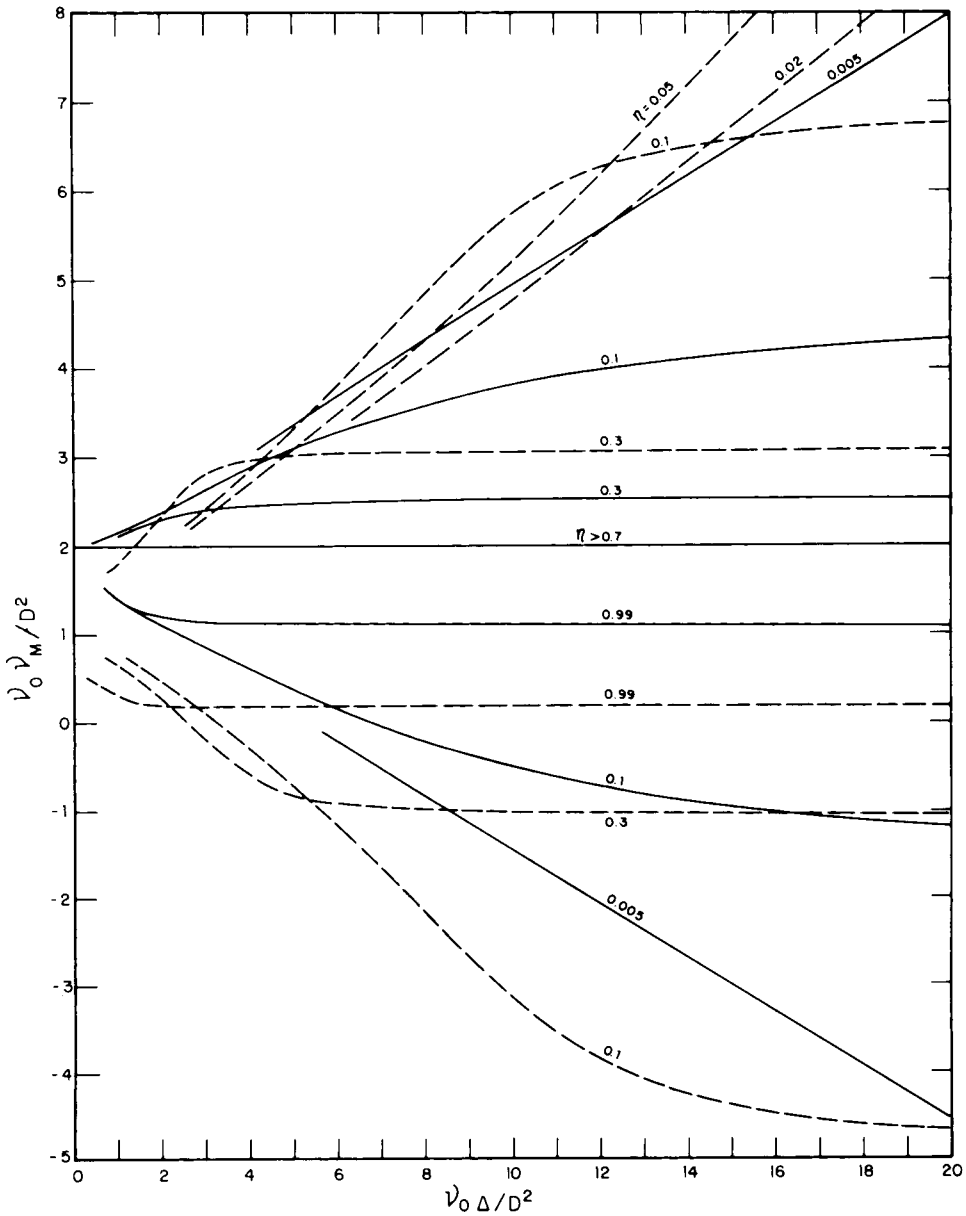

FIG 2. Frequency shifts of the perturbed lines. ν_M is the frequency shift of the maximum of the perturbed line measured from the central frequency ν_0 of the unperturbed line. D is defined in Table 1 and Δ is the full width at half maximum. The solid curves correspond to $\alpha = 0°$ and the dashed curves to $\alpha = 90°$. All curves drawn in the region above $\nu_0\nu_M/D^2 = 1.7$ correspond to ν_+ transitions, while those in the region below 1.7 correspond to ν_- transitions. All the plotted curves were calculated with $\Delta/\nu_0 = 1\times10^{-4}$. The curves with $\Delta/\nu_0 = 4\times10^{-4}$ were also calculated but they are very similar to the former and are not plotted.

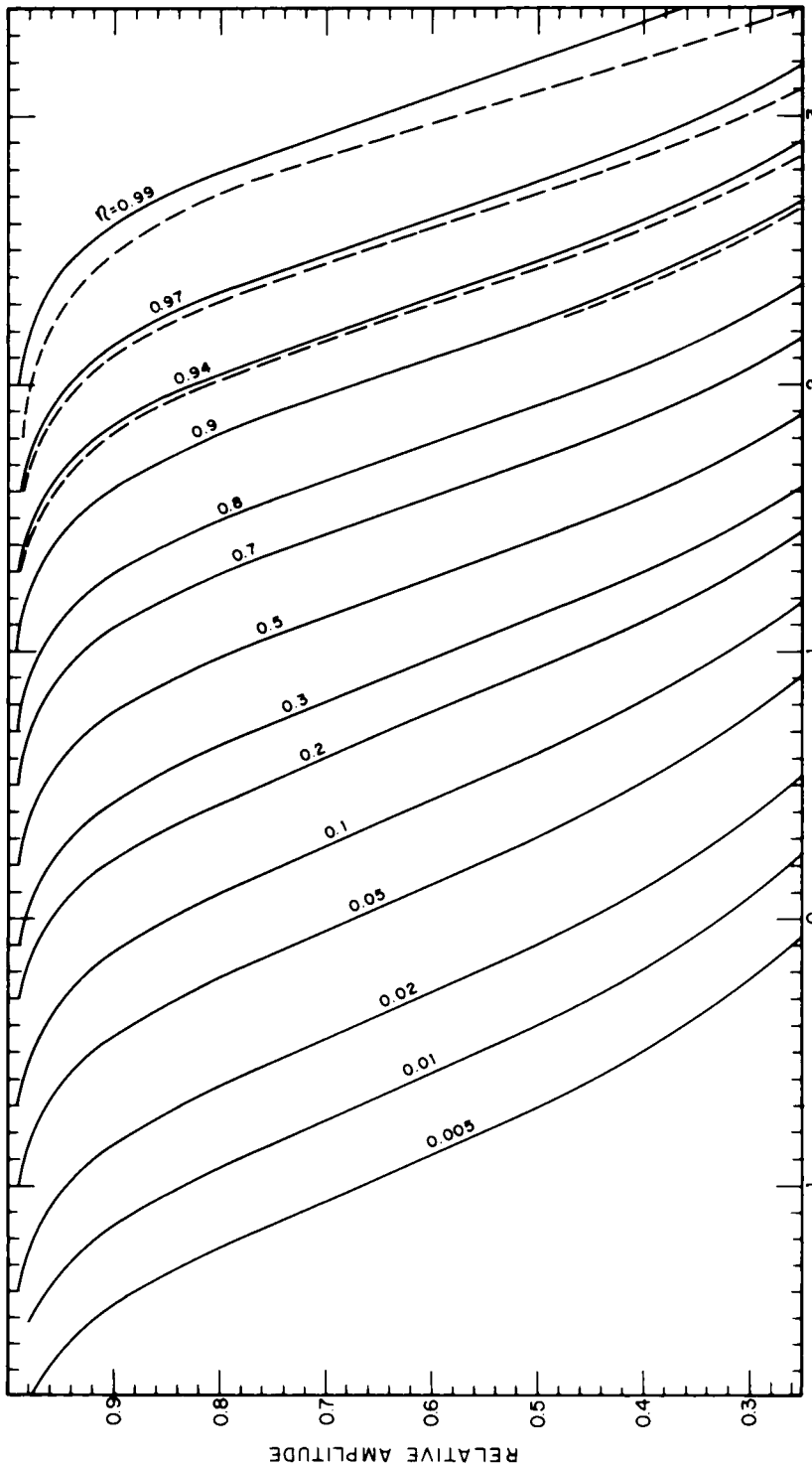

FIG. 3. The relative amplitudes of the ν_+ lines of a polycrystalline sample as functions of the Zeeman magnetic field H applied parallel to the radiofrequency magnetic field, for different values of the asymmetry parameter η. The solid curves correspond to $\Delta/\nu_0 = 1 \times 10^{-4}$ and the dashed curves to $\Delta/\nu_0 = 4 \times 10^{-4}$. The dashed curves were not drawn in most cases because they practically coincide with the solid curves.

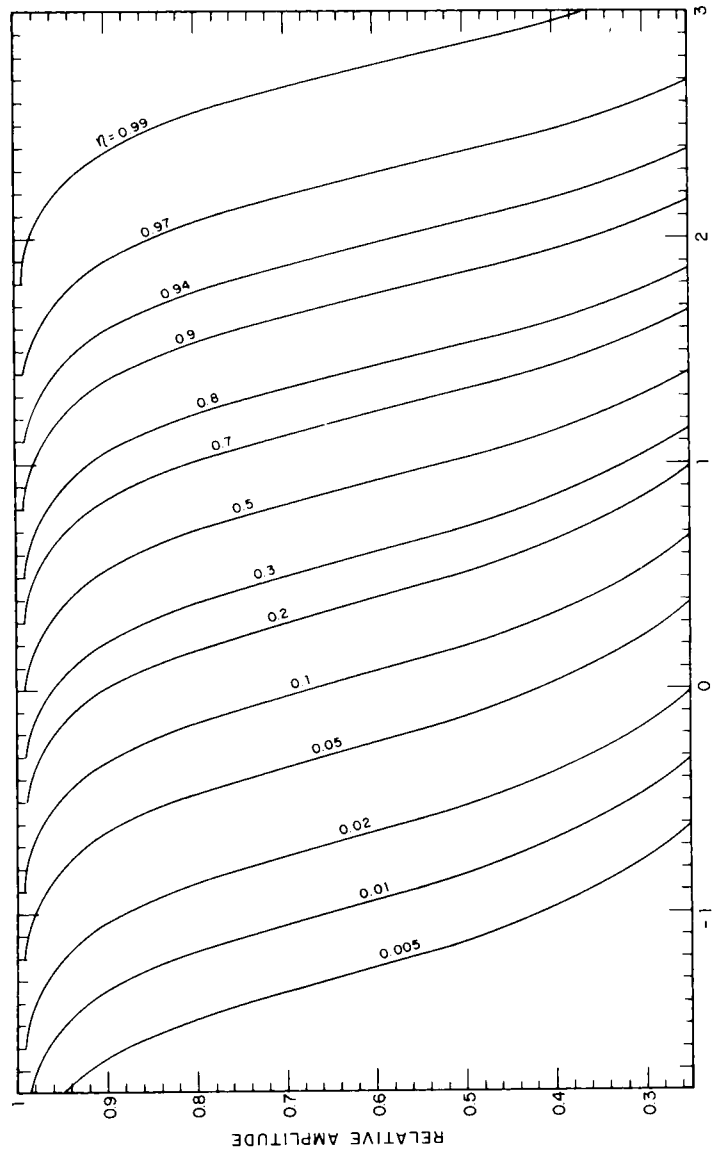

FIG. 4. The relative amplitudes of the ν_+ lines of a polycrystalline sample as functions of the Zeeman magnetic field H applied perpendicular to the radiofrequency magnetic field, for different values of the asymmetry parameter η. The same curves hold for $\Delta/\nu_0 = 1 \times 10^{-4}$ and $\Delta/\nu_0 = 4 \times 10^{-4}$.

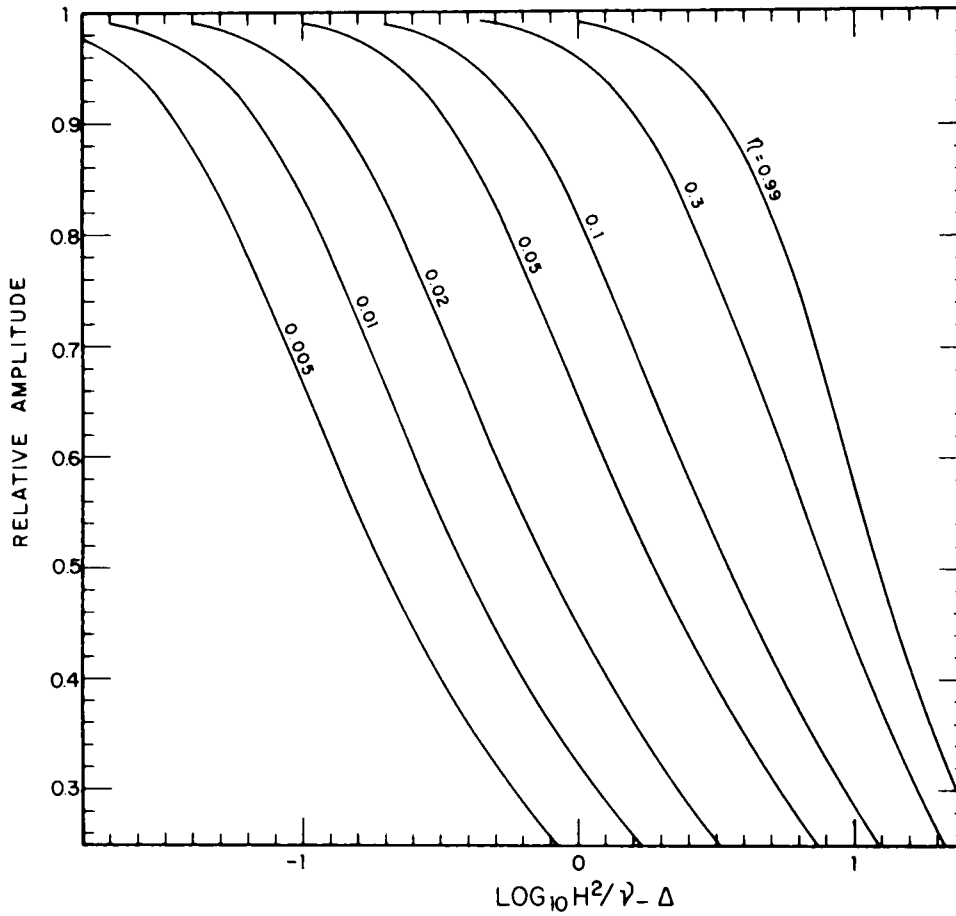

FIG. 5. The relative amplitudes of the ν_- lines of a polycrystalline sample as functions of the Zeeman magnetic field H applied parallel to the radiofrequency magnetic field, for different values of the asymmetry parameter η. The same curves hold for $\Delta/\nu_0 = 1 \times 10^{-4}$ and $\Delta/\nu_0 = 4 \times 10^{-4}$.

relative energies and amplitudes, and our result shows that the relative energy absorbed by the unperturbed line is equal to 1.

The total relative energy absorbed by the sample can also be calculated by integration of Eq. [33]:

$$P(\alpha) = \int_{\nu=\nu_{\min}}^{\nu_{\max}} P(\nu, \alpha)\, d\nu, \qquad [38]$$

where $\nu_{\min}$ and $\nu_{\max}$ are obtained by using Eq. [8] in Eqs. [11], and are given in Table 1 for each line in a nondimensional form.

The integration in Eq. [38] can only be carried out numerically, and the results should be compared with those obtained from the simple expressions [37]. This comparison serves two purposes. First, it is a critical test of the expressions of $P(\nu, \alpha)$ (we call it step 4). Second, it is an essential step for the determination of the

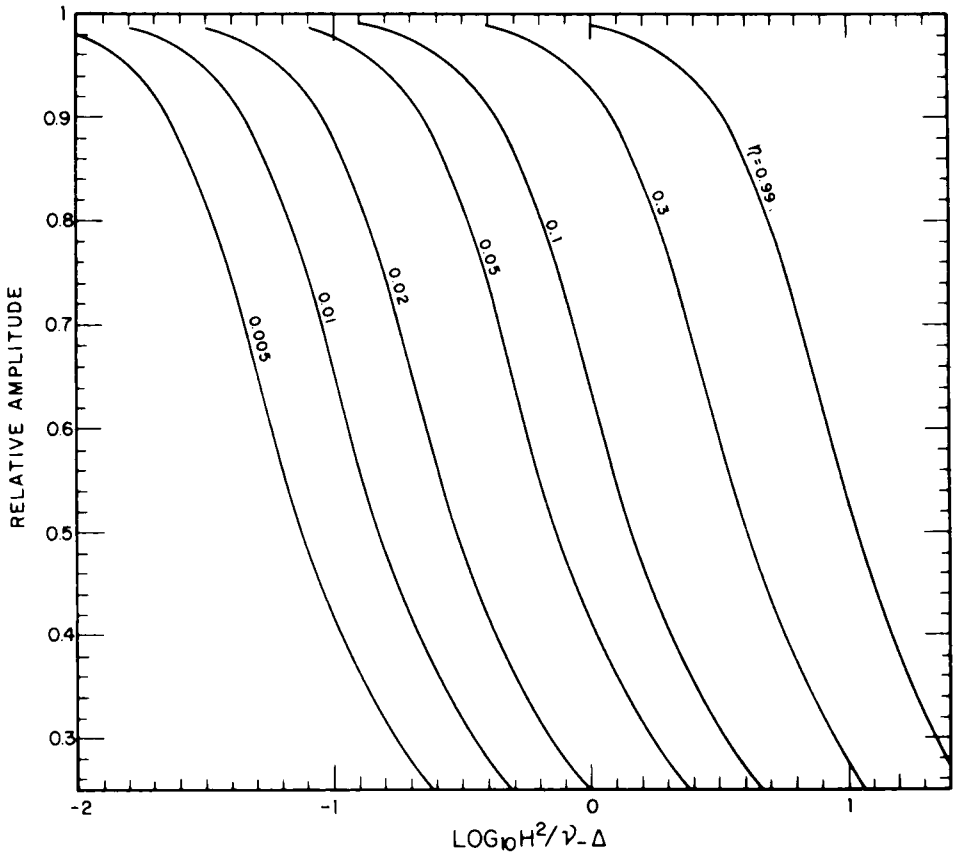

FIG. 6. The relative amplitudes of the ν_- lines of a polycrystalline sample as functions of the Zeeman magnetic field H applied perpendicular to the radiofrequency magnetic field, for different values of the asymmetry parameter. The same curves hold for $\Delta/\nu_0 = 1 \times 10^{-4}$ and $\Delta/\nu_0 = 4 \times 10^{-4}$.

parameters of the numerical integration which will be required when we deal with wide lines, Eq. [40].

We have compared numerically Eqs. [37] and [38] for 60 different pairs of values of α and η covering the entire range of interest for each of the three lines. The interval of integration in Eq. [38] corresponds to the range of values of v given by Eq. [8]. This range was subdivided in the three intervals $(0, \lambda - \varepsilon)$, $(\lambda - \varepsilon, \lambda + \varepsilon)$ and $(\lambda + \varepsilon, \lambda + 1)$, since the integrand diverges for $v = \lambda$. In the interval $(\lambda - \varepsilon, \lambda + \varepsilon)$ the integral was approximated, for ε sufficiently small. Each of the intervals $(0, \lambda - \varepsilon)$ and $(\lambda + \varepsilon, \lambda + 1)$ was divided in turn into N subintervals, and in each of the subintervals the integral was calculated by Gaussian integration of order 28. This required the calculation of the value of the integrand at 28 interior points and at both ends of each subinterval. The subintervals were not equal but decreased geometrically in the direction in which v approached λ, because the closer v to λ the steeper the function $P(\nu, \alpha)$ and the smaller the interval required for an accurate numerical integration. We call R the geometric factor. We have observed that the accuracy of the results increased as N increased and as R decreased. After several trials (with

TABLE 2

THE DESIGNATIONS OF THE INVESTIGATED NQR LINES, AND THEIR FREQUENCIES ν_0, ASYMMETRY PARAMETERS η, AND FULL WIDTHS AT HALF MAXIMUM $\Delta(1)$[a]

Compound	Line	Designation	ν_0 (kHz)	η	Δ (kHz)	Δ/ν_0
Acetonitrile	ν_+	A	2807.8	0.0046	0.87	3.10×10^{-4}
	ν_+	B	2810.8	0.0082	0.59	2.10
	ν_-	P	2799.2	0.0046	0.86	3.07
	ν_-	Q	2795.4	0.0082	0.58	2.07
3-Cyanopyridine	ν_+	C	3010.8	0.0999	0.70	2.32
	ν_+	D	3899.7	0.3667	0.75	1.92
	ν_-	R	2816.8	0.0999	0.53	1.88
	ν_-	S	3050.2	0.3667	0.50	1.64
Phenylhydrazine	ν_+	E	4909.6	0.616	0.94	1.91
	ν_+	F	4747.4	0.698	0.88	1.85
	ν_-	T	3236.5	0.616	0.70	2.16
	ν_-	U	2954.2	0.698	0.48	1.62
Diethylcyanamide	ν_+	G	2756.6	0.96	0.55	2.00

[a] Also given are the ratios Δ/ν_0.

double-precision Fortran) we achieved an accuracy of at least five figures in Eq. [38] with the selected values $N = 30$ and $R = 0.85$. Note that this required the calculation of $P(\nu, \alpha)$ from Eq. [33], 1742 times for each case, which took a great deal of computer time. The elliptic integrals were calculated by the well-known formulas of Hastings, of degree 7.

LINES WITH FINITE WIDTH

The study of the case of a real NQR absorption line having a certain width is the last step of this theory, or step 5. The following assumptions are made:

(iii) The factors which determine the shape of the unperturbed line do not change when the magnetic field is applied.

(iv) The shape of the unperturbed line can be described by the Gaussian function:

$$g(\nu/\Delta) = \exp\{-(4 \ln 2)(\nu/\Delta)^2\}, \qquad [39]$$

where Δ is the full width at half-maximum and ln stands for natural logarithm.

Under such assumptions, the shape of a real line perturbed by a Zeeman field, applied at an angle α with respect to the radiofrequency magnetic field, will be described by:

$$G(\nu, \Delta, \alpha) = \int_{\nu'=\nu_{\min}}^{\nu_{\max}} P(\nu', \alpha) g\{(\nu - \nu')/\Delta\}\, d\nu', \qquad [40]$$

where $\nu_{\min}$ and $\nu_{\max}$ are given in Table 1.

$G(\nu, \Delta, \alpha)$ should become identical with $g(\nu/\Delta)$ when $D = 0$. It does in fact, as can be easily proved by introducing the new variable of integration $\nu_0\nu'/D^2$ in Eq. [40]

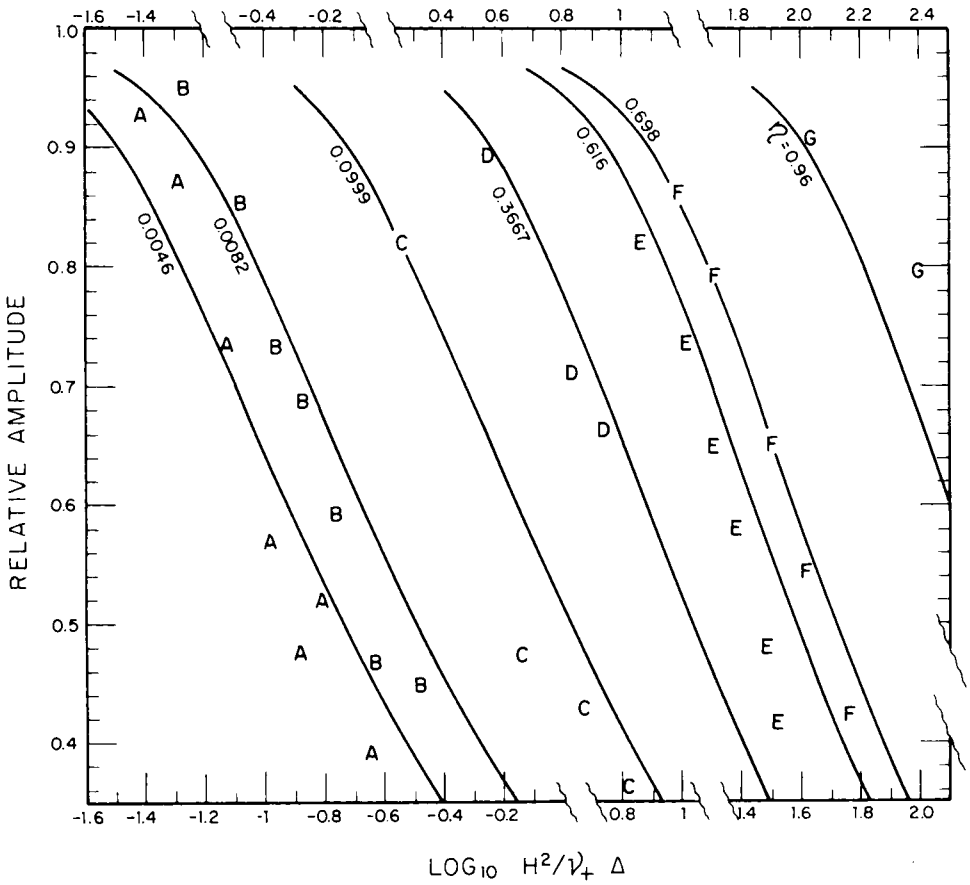

FIG. 7. Comparison of theory and experiment for ν_+ lines in the case $\alpha = 0°$. The theoretical curves were computed using the observed values of η and Δ/ν_+ of the NQR lines A, B, C, D, E, F, and G, which are identified in Table 2. The alphabetical characters represent experimental points measured for the same lines.

and noting that $\nu' = 0(D^2)$ when $D \to 0$ (see the definition of the limits of integration $\nu_{\min}$ and $\nu_{\max}$ in Table 1 and also Eq. [33]). Therefore, when $D \to 0$, then $\nu' \to 0$ and $g(\nu/\Delta)$ comes out of the integral, which takes the exact form of Eq. [38] and has a value of 1 for $D = 0$. This property of $G(\nu, \Delta, \alpha)$ is again a consequence of the fact that we are working with relative amplitudes, and has been achieved by the introduction of the constant $(8\pi^2/3)^{1/2}$ in Eqs. [20].

The integration in Eq. [40] can only be performed numerically. As the integrand is of the same type as that in Eq. [38], we have used the same values for the adjustable parameters N and R in order to obtain a similar accuracy.

DISCUSSION AND CONCLUSIONS

Equation [40] is the final result of this theory. By means of Eq. [40] it is possible to calculate the shape of a NQR absorption line of known asymmetry parameter η and

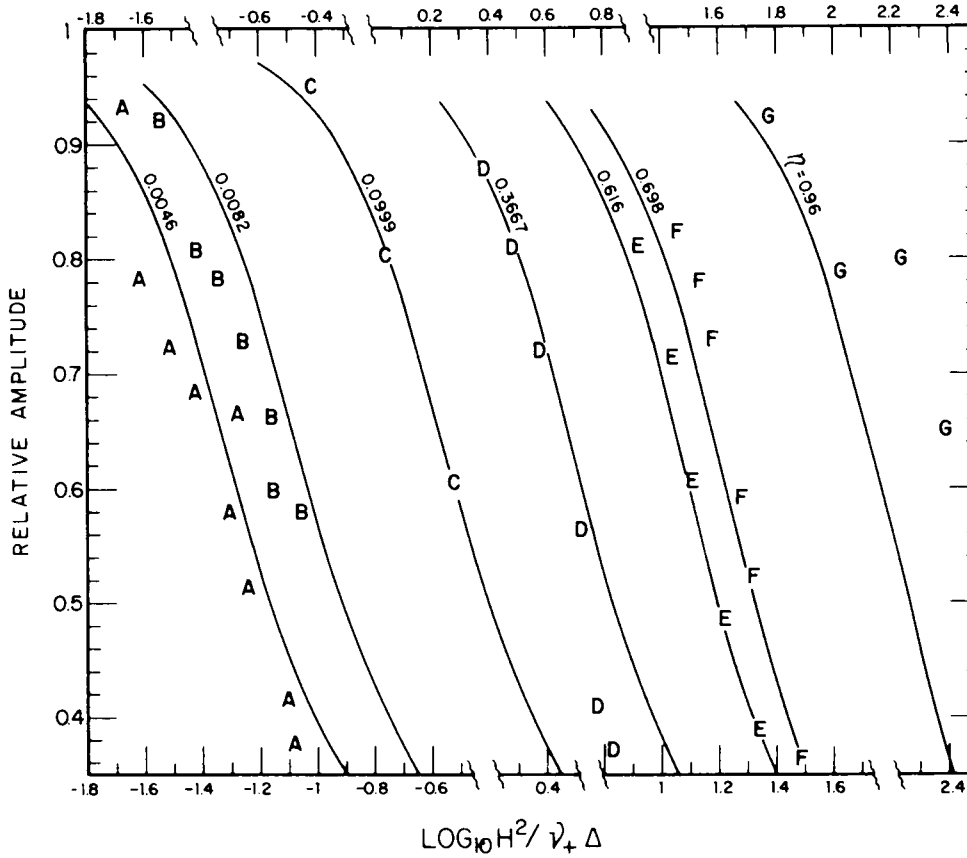

FIG. 8. Comparison of theory and experiment for ν_+ lines in the case $\alpha = 90°$. The theoretical curves were computed using the observed values of η and Δ/ν_+ of the NQR lines A, B, C, D, E, F, and G, which are identified in Table 2. The alphabetical characters represent experimental points measured for the same lines.

width Δ, when it is perturbed by a Zeeman magnetic field H applied at an angle α with respect to the radiofrequency magnetic field H'. Eq. [40] is valid for any value of α, $0 \leq \alpha \leq \pi/2$, and for η in the range $0.001 \ll \eta < 0.993$ (1).

Several sets of theoretical curves were computed using Eq. [40]. They are presented in Figs. 2–6. All the calculations are carried in terms of the dimensionless quantities:

$$\nu_0 \Delta/D^2 \quad \text{and} \quad \nu_0 \nu/D^2,$$

where D is defined in Table 1 and we use the value $g\mu_0/h = 308$ Hz/G. When Eq. [33] is used in Eq. [40], the factor D^2/ν_0^2 is written as

$$D^2/\nu_0^2 = (\Delta/\nu_0)/(\nu_0 \Delta/D^2).$$

The new experimental dimensionless parameter Δ/ν_0 is thus present in the theory. This parameter did not exist in the previous version (*1*). A practical range of values

for this parameter is:

$$1\times10^{-4}<\Delta/\nu_0<4\times10^{-4}$$

as shown in Table 2. All the theoretical curves were computed for the two cases: $\Delta/\nu_0=1\times10^{-4}$ and $\Delta/\nu_0=4\times10^{-4}$. However, in all but a few cases the results were found to be independent of Δ/ν_0 in this range and within the plotting accuracy. All curves are thus plotted for $\Delta/\nu_0=1\times10^{-4}$, except in Fig. 3, where curves are drawn for $\Delta/\nu_0=4\times10^{-4}$ when possible.

Only the shape of the perturbed line is given by Eq. [40] as a function of the frequency shift ν ($\nu=0$ at the center of the unperturbed line). Therefore, for each point in the plots, it was necessary to perform a numerical search of the maximum

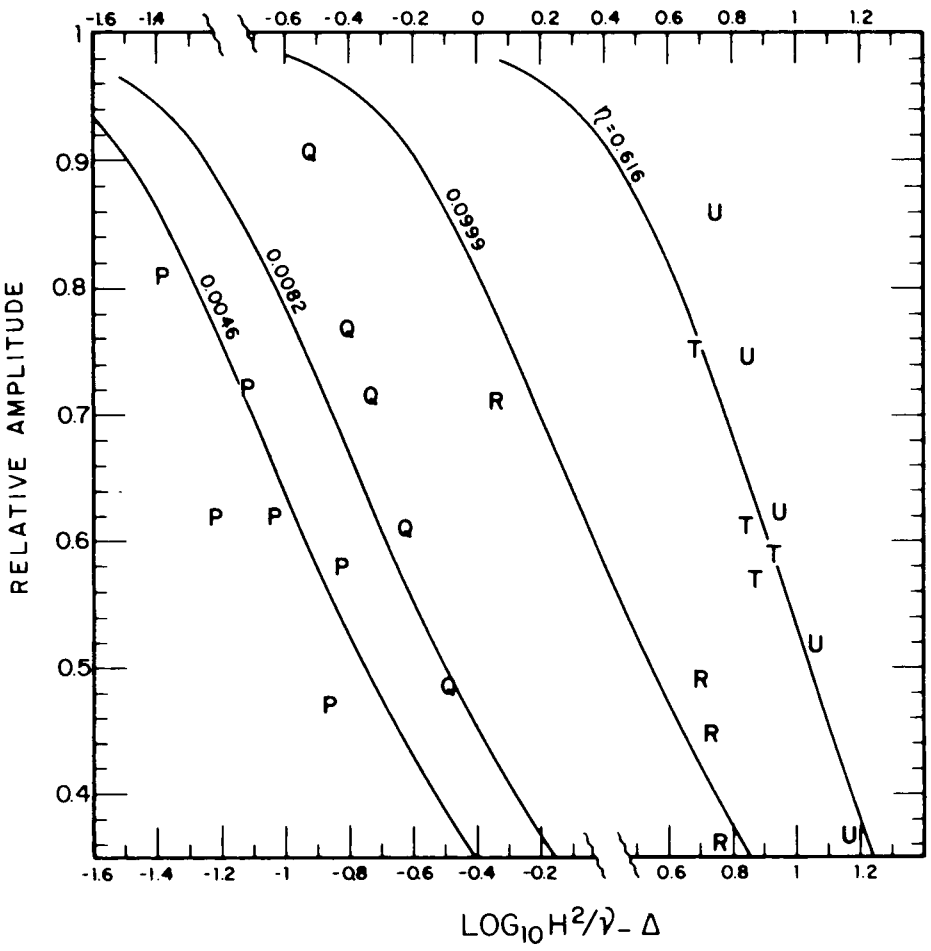

FIG. 9. Comparison of theory and experiment for ν_- lines in the case $\alpha=0°$. The theoretical curves were computed using the observed values of η and Δ/ν_- of the NQR lines P, Q, R, T, and U, which are identified in Table 2. The curve for line U was not represented because it is very close to the curve for line T. The alphabetical characters represent experimental points measured for the same lines.

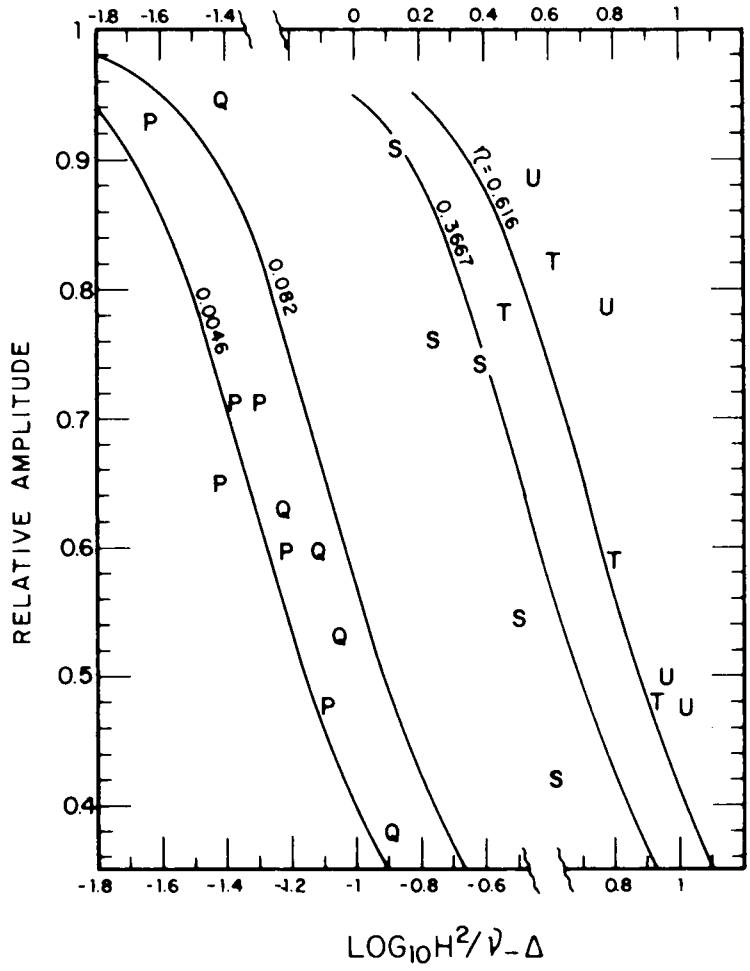

FIG. 10. Comparison of theory and experiment for ν_- lines in the case $\alpha = 90°$. The theoretical curves were computed using the observed values of η and Δ/ν_- of the NQR lines P, Q, S, T, and U, which are identified in Table 2. The curve for line U was not represented because it is very close to the curve for line T. The alphabetical characters represent experimental points measured for the same lines.

of the perturbed line. Both the frequency shift ν_M and the relative amplitude were determined at the maximum. The frequencies were plotted for some cases in Fig. 2. This plot is very similar to Fig. 5 of Ref. (*1*). In Ref. (*1*) we have made the comment that it did not seem possible to obtain good information concerning the value of the asymmetry parameter η from frequency shift measurements. This conclusion remains valid.

However, good values of η can be determined from amplitude measurements. The amplitudes at the maximum of the perturbed lines are plotted in Figs. 3–6. Figures 3 and 4 are for ν_+ lines and $\alpha = 0$ and $\pi/2$, respectively. The general features of these plots remain the same as in Ref. (*1*). However, there is an important difference: the fitting with the experimental results is largely improved. In order to make this fact

evident we have also computed the curves of relative amplitude for all the lines described in Table 2. The results are plotted in Figs. 7–10 and compared with the experimental data. In all cases the fitting is much better than previously. The curves are steeper and tend to represent quite effectively the steep descent of the experimental points.

The tendency of the upper points to fall in regions of too high η was mentioned in Ref. (*1*) and attributed to the strong dependence of the amplitude on the detailed lineshape for fields of the order of the critical field. This tendency is much smaller in the frame of this true-second-order theory. As an example, for the line A, with $\eta = 0.0046$, the upper points in Figs. 6 and 7 of Ref. (*1*) fall in regions of $\eta \simeq 0.015$ and $\eta \simeq 0.0075$, respectively, while in Figs. 7 and 8 of this paper they fall in regions of $\eta \simeq 0.007$ and $\eta \simeq 0.006$, respectively.

A single observed line can be identified to be a ν_+ or a ν_- with the help of Fig. 2. The required measurements are: the central frequency ν_0, the full width at half maximum Δ and the amplitude of the unperturbed line, and few measurements of the frequency shifts ν_M vs the magnetic field H at the maximum of the perturbed line. All these measurements can be easily done on the usual records which are obtained with a cw spectrometer. Once the line has been identified, the same records can be used to obtain values of the amplitude at the maximum of the perturbed line, and then determine a good value of η with the help of Figs. 3–6. Of course, for ν_- lines, the resolution is very poor if $\eta > 0.3$.

The results we have presented here are thus the basis for the identification of lines and for the measurement of the asymmetry parameter when a single line is observed or when several lines are observed and have to be paired.

REFERENCES

1. S. PISSANETZKY, *J. Chem. Phys.* **59,** 4197 (1973).
2. H. KRUGER, *Z. Physik* **130,** 371 (1951).
3. P. A. CASABELLA AND P. J. BRAY, *J. Chem. Phys.* **28,** 1182 (1958).